THE JOURNAL OF PHYSICAL CHEMISTRY Letters

Letter

Cite This: J. Phys. Chem. Lett. 2018, 9, 6399−6403

pubs.acs.org/JPCL

Comparing Geometry and Chemistry When Confined Molecules Diffuse in Monodisperse Metal−Organic Framework Pores

Ah-Young Jee,[†] Nobuhiro Yanai,[‡] and Steve Granick*[,†,§]

[†]Center for Soft and Living Matter, Institute for Basic Science (IBS), Ulsan 44919, South Korea

[‡]Department of Chemistry and Biochemistry, Graduate School of Engineering, Center for Molecular Systems (CMS), Kyushu Universityy, 744 Moto-oka, Nishi-ku, Fukuoka 819-0395, Japan

[§]Department of Chemistry, Ulsan National Institute of Science and Technology (UNIST), Ulsan 44919, South Korea

Supporting Information

ABSTRACT: The monodisperse pore structure of MOFs (metal−organic frameworks) is advantageous for investigating how porosity influences diffusion. Here we report translational and rotational diffusion using fluorescence correlation spectroscopy and time-correlated single-photon counting, using the three-dimensional pores of the zeolitic-like metal−organic framework family. We compare the influence of size and electric charge as well as dependence on pore size that we controlled through postsynthetic cation-exchange modifications. Charge−charge interactions with the MOF appeared to produce transient adsorption, manifested as a relatively fast and a slower diffusion process, but diffusants without net electric charge displayed a single diffusion process. Obtained from this family of guest molecules selected to be fluorescent, these findings suggest potentially useful general design rules to predict how pore size, guest size, and host−guest interaction control guest mobility within nanopores. With striking fidelity, diffusion coefficient scales with the ratio of cross-sectional areas of diffusant and host pores when charge is taken into account.

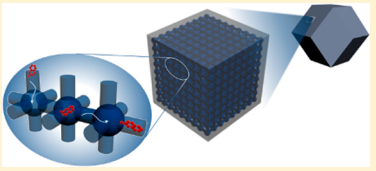

The diffusion of guest molecules within nanoporous metal−organic framework (MOF) materials is fundamental to their properties and applications, among them storage, exchange, separation, release, and catalysis.[1−11] However, diffusivity might in principle be contingent on a myriad of parameters, among them pore size, pore dimensionality, and host−guest interaction;[12−15] therefore, here we have endeavored to formulate general conclusions regarding the interplay of geometrical structure and specific chemical interactions in this model system. Indeed, molecular diffusion in nano- and microporous materials can be quantified by numerous techniques, including pulsed field gradient NMR,[2,16−18] quasi-elastic neutron scattering, quartz-crystal microbalance,[19−21] microimaging using interference microscopy, and IR microscopy,[22−27] but these tend to suffer from a lack of spatial resolution, unlike the experiments described below. The desirable resolving of the inconsistency between earlier reported results in which diffusion was sometimes relatively rapid[3] and sometimes nearly quenched in a three-dimensional (3D) nanoporous system[28] was achieved here by making measurements within the same system of what happens when both pore size and host−guest interaction are varied systematically. Furthermore, for what is considered to be the first time in a MOF system, we compare translational with rotational diffusion.

MOFs were selected because their pore matrix is regular, while their pore size and chemical makeup can be precisely tailored by adjusting counterions within the ionic frameworks and modifying frameworks with functional groups.[8,29−37] We selected the anionic zeolitic-like metal−organic framework (ZMOF)[22,38] because of the ease of forming large crystals and its homogeneous three-dimensional pore structure. Importantly, this system offers the capacity to tune pore size according to its cation-exchange capacity. This ZMOF system, $|X_n|[In_{48}(HImDC)_{96}]$ (X = countercation; HImDC = partially deprotonated form of 4,5-imidazoledicarboxylic acid) contains large rectilinear cavities of 1.8 nm radius connected by windows of ca. 0.9 nm radius.[22,38] Therefore, diffusion of guest species can be studied within sample geometry that is defined with precision. To this end, we synthesized ZMOF materials having protonated forms of 1,3,4,6,7,8-hexahydro-2H-pyrimido[1,2-*a*]pyrimidine (HPP) and dimethyl amine (DMA) as counter cations, denoted as HPP-ZMOF and DMA-ZMOF, respectively. The procedures were described previously.[22] The frameworks containing Na^+ ions and Na-ZMOF were obtained by cation exchange using DMA-ZMOF as the parent framework.[22] The composition and structure of these materials were confirmed by elemental analysis and X-ray powder diffraction measurements (Table S1 and Figure S1). Although locations can vary within the framework depending on the cation type, the representative Mg-ZMOF structure shows the location of the cation in this case (Figure S2). From scanning electron microscopy (SEM) measurements, all samples showed the expected rhombic dodecahedron morphology. The large crystal sizes (Figure S3) were an important design feature as they enabled us to carry out optical

Received: September 12, 2018
Accepted: October 23, 2018

DOI: 10.1021/acs.jpclett.8b02810
J. Phys. Chem. Lett. 2018, 9, 6399−6403

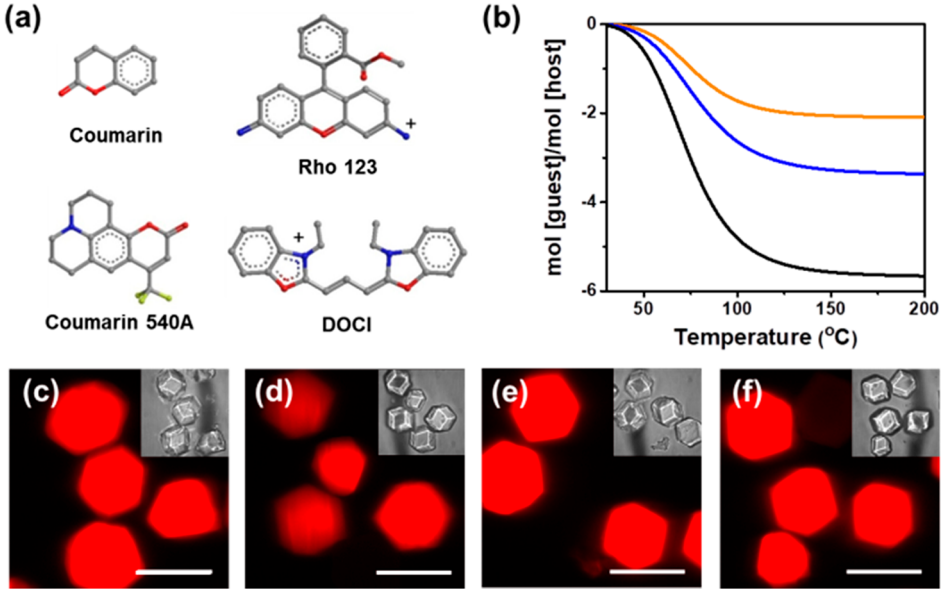

Figure 1. Guest molecules and their inclusion within MOF structures. (a) Molecular structure of diffusing molecules: coumarin, coumarin 540A, rhodamine 123 (Rho 123), and 3,3-diethyloxacarboxyanine iodide (DOCI). (b) Thermogravimetric analysis (TGA) traces of the ZMOF hosts after exposure to 1-butanol vapor at room temperature, where black, blue, and orange show data in Na-, DMA-, and HPP-ZMOF, respectively. Confocal microscopy images of the HPP-ZMOF crystals encapsulating (c) coumarin, (d) coumarin 540A, (e) DOCI, and (f) Rho 123 in DMF show that the diffusants occupied the framework volume uniformly. Scale bars = 50 μm. Insets show bright field optical microscopy images of these same samples with magnification 2.5 times less.

experiments safely within the diffraction-based size (~300 nm diameter) of a focused laser beam needed to perform this characterization.

To examine how counter cations modulate the pore size, we performed thermogravimetric analysis (TGA) of the three materials, HPP-ZMOF, DMA-ZMOF, and Na-ZMOF. Host crystals were dried and exposed to 1-butanol vapor at room temperature. Weight losses up to 150 °C of 2.13, 3.36, and 5.65 mol/mol were observed for HPP-, DMA-, and Na-ZMOFs, respectively (Figure 1b). Considering the cation size (Figure S4), it is consistent that the guest loading amounts grew with increasingly larger pore size of the ZMOF materials (relative pore sizes: HPP-ZMOF < DMA-ZMOF < Na-ZMOF). Pore size distributions were obtained by analyzing nitrogen adsorption isotherms using a density functional theory (DFT) analysis method.[39] The N_2 isotherms measured for these ZMOFs and the inferred pore size distributions (PSD) were 9.2, 11.5, and 13.2 Å for HPP-, DMA-, and Na-ZMOF, respectively (Figures S5 and Figure S6). The large size of the cavities is the overall negative charge of the cavity interior, so exchange and incorporation by cationic organic molecules occurs mainly in the large cavity.[40] Accordingly, the observed difference in average measured pore size mainly reflects the different size of the pore cavity rather than the pore window.

For initial choice of guest molecule, we began with coumarin, a fluorescent molecule whose neutral charge was anticipated to produce minimal electrostatic interaction with the net negative charge of the pores within which it migrated. Its relatively small size, thickness of ~0.62 nm in the short direction, was an additional reason to select this system. To prepare samples, first the ZMOF crystals were soaked in a 1 nM DMF solution of coumarin for 48 h; the crystals were then rinsed with DMF several times. Confocal microscopy images showed that coumarin molecules became distributed homogeneously within the host crystals (Figure 1c).

The measurements employed fluorescence correlation spectroscopy (FCS), a technique based on measuring fluctuations in the number of fluorescent molecules within a small illumination volume.[3,41,42] From inspection of intensity–intensity autocorrelation functions, translational diffusion coefficient can be deduced. For three different hosts, the autocorrelation curves in Figure 2a illustrate diffusion of coumarin, the diffusion coefficient increasing almost exponentially with increasing pore size (Figure 2b) but in every case retarded by more than 2 orders of magnitude relative to this molecule's diffusion coefficient in DMF solution (375 $\mu m^2 s^{-1}$). The same pattern holds for coumarin 540A, whose hydrodynamic size is larger (~0.84 nm), whose electrical charge is neutral, and for which rotational anisotropy measurements presented below demonstrate that host–guest interaction does not play a major role. For these dyes, the influence of pore size dominates.

Exploring the role of electric charge, we compared the diffusion of cationic fluorescent dyes 3,3-diethyloxacarboxyanine iodide (DOCI) and rhodamine 123 (Rho 123), which experience electrostatic attraction to the anionic host frameworks. Evaluated using ChemDraw, the molecular size of DOCI is 0.97 nm in the long axis and 0.38 nm in the short axis; for Rho 123, these numbers are 0.84 nm and 0.87 nm, respectively. Both diffusants could enter all three ZMOF frameworks as their size in the short axis is less than the pore size, and we confirmed from fluorescence imaging that they occupied the framework volume uniformly (Figure 1e,f). The autocorrelation curves of DOCI were composed of two well-separated components, fast and slow (Figure 2c), as can be seen from inspecting residuals of fits (Figure 2c inset). Two-component fitting was similarly needed for the other cationic diffusant, Rho 123. Diffusion coefficients increased with

DOI: 10.1021/acs.jpclett.8b02810
J. Phys. Chem. Lett. 2018, 9, 6399–6403

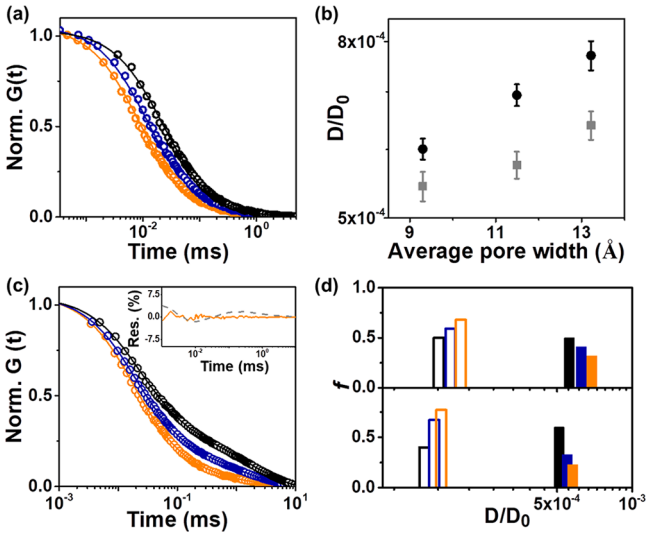

Figure 2. (a) Intensity−intensity autocorrelation functions $G(t)$, normalized to unity at short times, plotted against lag time for the electrically neutral molecule, coumarin, in HPP-ZMOF (black), DMA-ZMOF (blue), and Na-ZMOF (orange). Lines through the data are fits to the model of a simple, one-component diffusion process. (b) The implied translational diffusion coefficients, divided by diffusion coefficient (D_0) in DMF, are plotted for coumarin (black) and coumarin 540A (gray) in the three host systems. (c) For the cationic molecule DOCI, normalized autocorrelation function $G(t)$ is plotted in the same host systems. Two-component diffusion is needed, as illustrated by the inset showing the fit residual for one-component (dotted line) and two-component (solid line) fitting of the curve in HPP-ZMOF. (d) The implied two-component diffusion coefficients (D), normalized to diffusion D_o in DMF solution, for DOCI (upper panel) and a second cationic molecule, Rho 123 (lower panel), for HPP-ZMOF (black), DMA-ZMOF (blue), and Na-ZMOF (orange).

increasing pore size, in qualitative agreement with findings for the electrically neutral diffusants, but strikingly, despite having similar diffusion coefficients in solution (DOCI of 282 $\mu m^2\ s^{-1}$ and Rho 123 of 270 $\mu m^2\ s^{-1}$ in DMF), this was violated inside the MOF pores. Figure 2d shows that the skinnier molecule diffused more rapidly.

We introduce the dimensionless ratio of cross-sectional areas A_H/A_G in which A_G and A_H are the cross sections of the guest molecule and host pore, respectively. The quantity A_G was inferred from the square of the hydrodynamic radius by measuring the diffusion coefficient in DMF and inferring the hydrodynamic radius from Stokes' law, $D = k_BT/6\pi\eta A_G$, where k_B is the Boltzmann constant, D the diffusion coefficient in pure DMF, and η viscosity. These measurements gave $R = 0.62$ nm (coumarin), 0.80 nm (coumarin 540A), 0.84 nm (DOCI), and 0.87 nm (Rho 123). Figure 3 plots D/D_0, the diffusion coefficient normalized by its value in DMF solution, as a function of this measure of geometrical confinement. We find that diffusion of the neutral molecules (coumarin and coumarin 540A) and the fast diffusion coefficient of the cationic molecules (DOCI and Rho123) fall empirically on the same power-law curve. The slow-component diffusion of the cationic molecules appears to follow a power law with the same slope, but slower by a factor of 3, where this slower process presumably quantifies the intensity of electrostatic attraction to the framework. It is striking that both curves appear to follow

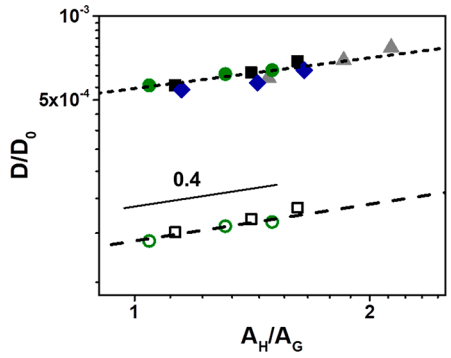

Figure 3. Diffusion coefficient D, normalized by diffusion coefficient D_0 in DMF solution, plotted against the ratio of cross-sectional areas of the diffusant and host pore, A_H/A_G, A_G and A_H, respectively, as explained in the text. The diffusion of coumarin (gray) and coumarin 540A (blue) and the fast diffusion components of DOCI (solid black) and Rho123 (solid green) fall on the same empirical power law with slope 0.40. The slow component for DOCI (empty black squares) and Rho123 (empty green circles) fall on the same empirical power law but slower by a factor of 3.

the same power law with slope 0.4, but we offer at this time no explanation of this number.

It is natural to anticipate that rotational diffusion might similarly be influenced by confinement and electrostatic interaction. Therefore, for deeper understanding, we measured the time-resolved fluorescence anisotropy of these same guest molecules after exciting them at 80 MHz with a femotosecond laser. According to the usual method of this technique, fluorescence decay was monitored parallel and perpendicular to the excitation polarization, giving time-dependent fluorescence $I_{\parallel}(t)$ and $I_{\perp}(t)$, respectively, after excitation by a vertically polarized laser beam. Panels a and b of Figure 4 compare raw data for a neutral molecule (coumarin) and a

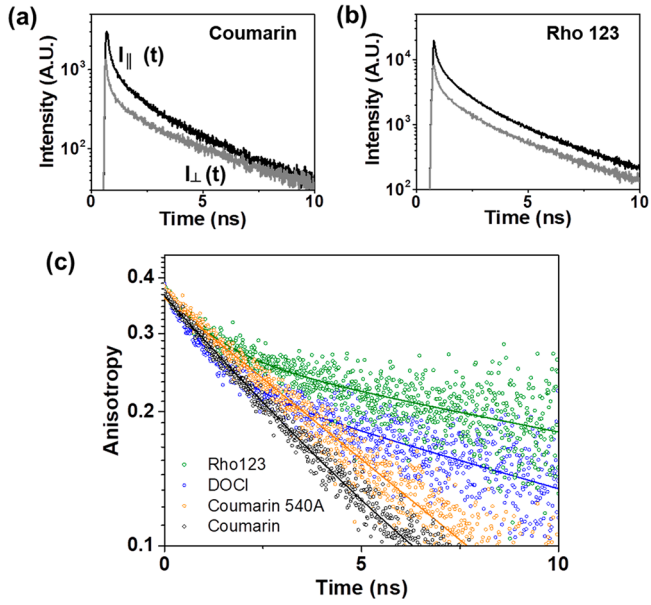

Figure 4. Fluorescence intensity decays of (a) coumarin and (b) Rho 123 in HPP-ZMOF. Polarized intensity in orthogonal directions ($I_{\parallel}$, parallel polarization; $I_{\perp}$, perpendicular polarization) is plotted semilogarithmically against time. (c) Time-resolved anisotropy decay of dyes in HPP-ZMOF.

DOI: 10.1021/acs.jpclett.8b02810
J. Phys. Chem. Lett. 2018, 9, 6399−6403

charged molecule (Rho 123) in HPP-ZMOF, respectively, and the difference is obvious to the eye. For the neutral molecule, the intensities of parallel and perpendicular fluorescence nearly coincide after only 10 ns, but not for the charged molecule. Evidently, rotation of the charged molecule was hindered, reflecting the influence of electrostatic attraction to the pores.

For quantification, Figure 4c shows the time-resolved anisotropy plotted against time in HPP-ZMOF. Anisotropy r is defined as

$$r(t) = \frac{I_{\parallel}(t) - I_{\perp}(t)}{I_{\parallel}(t) + 2I_{\perp}(t)} \quad (1)$$

For the neutral molecule (coumarin), regardless of the ZMOF, all the decay curves are nicely consistent with a single-exponential decay with time constant τ, the average rotational correlation time. The single-exponential decay suggests free rotation in the pore and no specific binding to the pore wall, but it is slightly more rapid with increasing pore size (Table S2) and 1 order of magnitude slower than for this same dye in free DMF solution. This tendency is also observed for coumarin 540A. Thus, not only translational diffusion but also rotational diffusion is controllable by changing the framework counterion. However, the charged molecules show a biexponential decay instead (Figure 4c). The slower rotational decay time increases to more than 20 ns, and this value is also affected by confinement as the pore size decreases (Table S2). These times, much slower than for the neutral molecules, probably reflect electrostatic attraction to the host framework, while the more rapid rotational decay times of the charged molecules probably reflect molecules that are in less intimate contact with the pore walls.

In summary, earlier important studies of ion-exchangeable MOFs focused on their adsorption properties, while concerns about guest mobility dwelt on macroscopic measurements such as the rate at which guests could be loaded or removed. The quantitative measurements presented here with the spatial resolution of a diffraction-limited focused laser spot (~300 nm) have revealed that translational and rotational diffusion vary with regularity according to pore size and guest charge. The remarkably regular patterns described here may assist rational improvement of various functions when molecular guests are loaded into MOFs.

■ ASSOCIATED CONTENT

Supporting Information

The Supporting Information is available free of charge on the ACS Publications website at DOI: 10.1021/acs.jpclett.8b02810.

Experimental procedures and characterization methods (PDF)

■ AUTHOR INFORMATION

Corresponding Author

*E-mail: sgranick@ibs.re.kr.

ORCID

Nobuhiro Yanai: 0000-0003-0297-6544

Steve Granick: 0000-0003-4775-2202

Notes

The authors declare no competing financial interest.

■ ACKNOWLEDGMENTS

This work was supported by the taxpayers of South Korea through the Institute for Basic Science, project code IBS-R020-D1. N.Y. acknowledges the support of JSPS KAKENHI (JP17H04799). We thank Sung Chul Bae for participation in early phases of this study.

■ REFERENCES

(1) Davis, B. H.; Sing, K. S.; Schüth, F.; Levitz, P. E.; Neimark, A. V.; Tesche, B.; Ramsay, J. D.; Pikunic, J.; Lastoskie, C. M.; Gubbins, K. E. *Handbook of Porous Solids*; Wiley-VCH: Weinheim, 2002.

(2) Stallmach, F.; Gröger, S.; Künzel, V.; Kärger, J.; Yaghi, O.; Hesse, M.; Müller, U. NMR Studies on the Diffusion of Hydrocarbons on the Metal-Organic Framework Material MOF-5. *Angew. Chem., Int. Ed.* **2006**, *45*, 2123−2126.

(3) Han, S.; Hermans, T. M.; Fuller, P. E.; Wei, Y.; Grzybowski, B. A. Transport into Metal−Organic Frameworks from Solution is not Purely Diffusive. *Angew. Chem.* **2012**, *124*, 2716−2720.

(4) Luo, F.; Yan, C.; Dang, L.; Krishna, R.; Zhou, W.; Wu, H.; Dong, X.; Han, Y.; Hu, T.-L.; O'Keeffe, M.; et al. UTSA-74: A MOF-74 Isomer with Two Accessible Binding Sites per Metal Center for Highly Selective Gas Separation. *J. Am. Chem. Soc.* **2016**, *138*, 5678−5684.

(5) Byun, J.; Patel, H. A.; Thirion, D.; Yavuz, C. T. Charge-Specific Size-Dependent Separation of Water-Soluble Organic Molecules by Fluorinated Nanoporous Networks. *Nat. Commun.* **2016**, *7*, 13377.

(6) Wang, C.; Lin, W. Diffusion-Controlled Luminescence Quenching in Metal−Organic Frameworks. *J. Am. Chem. Soc.* **2011**, *133*, 4232−4235.

(7) Han, S.; Wei, Y.; Valente, C.; Lagzi, I.; Gassensmith, J. J.; Coskun, A.; Stoddart, J. F.; Grzybowski, B. A. Chromatography in a Single Metal−Organic Framework (MOF) Crystal. *J. Am. Chem. Soc.* **2010**, *132*, 16358−16361.

(8) Li, J.-R.; Kuppler, R. J.; Zhou, H.-C. Selective Gas Adsorption and Separation in Metal−Organic Frameworks. *Chem. Soc. Rev.* **2009**, *38*, 1477−1504.

(9) Zacher, D.; Shekhah, O.; Wöll, C.; Fischer, R. A. Thin Films of Metal−Organic Frameworks. *Chem. Soc. Rev.* **2009**, *38*, 1418−1429.

(10) Ramaswamy, P.; Wong, N. E.; Shimizu, G. K. H. MOFs as Proton Conductors − Challenges and Opportunities. *Chem. Soc. Rev.* **2014**, *43*, 5913−5932.

(11) Bosch, M.; Yuan, S.; Rutledge, W.; Zhou, H.-C. Stepwise Synthesis of Metal−Organic Frameworks. *Acc. Chem. Res.* **2017**, *50*, 857−865.

(12) Ozin, G. A.; Kuperman, A.; Stein, A. Advanced Zeolite, Materials Science. *Angew. Chem., Int. Ed. Engl.* **1989**, *28*, 359−376.

(13) Davis, M. E. Ordered Porous Materials for Emerging Applications. *Nature* **2002**, *417*, 813.

(14) Wu, D.; Hwang, S.-J.; Zones, S. I.; Navrotsky, A. Guest−Host Interactions of a Rigid Organic Molecule in Porous Silica Frameworks. *Proc. Natl. Acad. Sci. U. S. A.* **2014**, *111*, 1720−1725.

(15) Lu, Z.; Godfrey, H. G.; Da Silva, I.; Cheng, Y.; Savage, M.; Tuna, F.; McInnes, E. J.; Teat, S. J.; Gagnon, K. J.; Frogley, M. D.; et al. Modulating Supramolecular Binding of Carbon Dioxide in R redox-Active Porous Metal-Organic Framework. *Nat. Commun.* **2017**, *8*, 14212.

(16) Taylor, J. M.; Mah, R. K.; Moudrakovski, I. L.; Ratcliffe, C. I.; Vaidhyanathan, R.; Shimizu, G. K. H. Facile Proton Conduction via Ordered Water Molecules in a Phosphonate Metal−Organic Framework. *J. Am. Chem. Soc.* **2010**, *132*, 14055−14057.

(17) Valiullin, R.; Kärger, J.; Gläser, R. Correlating Phase Behaviour and Diffusion in Mesopores: Perspectives Revealed by Pulsed Field Gradient NMR. *Phys. Chem. Chem. Phys.* **2009**, *11*, 2833−2853.

(18) Ford, D. C.; Dubbeldam, D.; Snurr, R. Q.; Künzel, V.; Wehring, M.; Stallmach, F.; Kärger, J.; Müller, U. Self-Diffusion of Chain Molecules in the Metal−Organic Framework IRMOF-1: Simulation and Experiment. *J. Phys. Chem. Lett.* **2012**, *3*, 930−933.

DOI: 10.1021/acs.jpclett.8b02810
J. Phys. Chem. Lett. 2018, 9, 6399−6403

(19) Rosenbach, N., Jr; Jobic, H.; Ghoufi, A.; Salles, F.; Maurin, G.; Bourrelly, S.; Llewellyn, P. L.; Devic, T.; Serre, C.; Férey, G. Quasi-Elastic Neutron Scattering and Molecular Dynamics Study of Methane Diffusion in Metal Organic Frameworks MIL-47 (V) and MIL-53 (Cr). *Angew. Chem., Int. Ed.* **2008**, *47*, 6611−6615.
(20) Salles, F.; Jobic, H.; Ghoufi, A.; Llewellyn, P. L.; Serre, C.; Bourrelly, S.; Férey, G.; Maurin, G. Transport Diffusivity of CO2 in the Highly Flexible Metal−Organic Framework MIL-53 (Cr). *Angew. Chem.* **2009**, *121*, 8485−8489.
(21) Zybaylo, O.; Shekhah, O.; Wang, H.; Tafipolsky, M.; Schmid, R.; Johannsmann, D.; Wöll, C. A Novel Method to Measure Diffusion Coefficients in Porous Metal−Organic Frameworks. *Phys. Chem. Chem. Phys.* **2010**, *12*, 8092−8098.
(22) Nouar, F.; Eckert, J.; Eubank, J. F.; Forster, P.; Eddaoudi, M. Zeolite-Like Metal−Organic Frameworks (ZMOFs) as Hydrogen Storage Platform: Lithium and Magnesium Ion-Exchange and H2-(rho-ZMOF) Interaction Studies. *J. Am. Chem. Soc.* **2009**, *131*, 2864−2870.
(23) Ramaswamy, P.; Wong, N. E.; Shimizu, G. K. MOFs as Proton Conductors−Challenges and Opportunities. *Chem. Soc. Rev.* **2014**, *43*, 5913−5932.
(24) Chmelik, C.; Kärger, J. Imaging of Transient Guest Profiles in Nanoporous Host Materials: a New Experimental Technique to Study Intra-Crystalline Diffusion. *Adsorption* **2010**, *16*, 515−523.
(25) Chmelik, C.; Kärger, J.; Wiebcke, M.; Caro, J.; Van Baten, J.; Krishna, R. Adsorption and Diffusion of Alkanes in CuBTC Crystals Investigated Using Infra-Red Microscopy and Molecular Simulations. *Microporous Mesoporous Mater.* **2009**, *117*, 22−32.
(26) Heinke, L.; Tzoulaki, D.; Chmelik, C.; Hibbe, F.; van Baten, J. M.; Lim, H.; Li, J.; Krishna, R.; Kärger, J. Assessing Guest Diffusivities in Porous Hosts from Transient Concentration Profiles. *Phys. Rev. Lett.* **2009**, *102*, 065901.
(27) Kärger, J.; Ruthven, D. M. Diffusion in Nanoporous Materials: Fundamental Principles, Insights and Challenges. *New J. Chem.* **2016**, *40*, 4027−4048.
(28) Liao, Y.; Yang, S. K.; Koh, K.; Matzger, A. J.; Biteen, J. S. Heterogeneous Single-Molecule Diffusion in One-, Two-, and Three-Dimensional Microporous Coordination Polymers: Directional, Trapped, and Immobile Guests. *Nano Lett.* **2012**, *12*, 3080−3085.
(29) Yaghi, O. M.; O'keeffe, M.; Ockwig, N. W.; Chae, H. K.; Eddaoudi, M.; Kim, J. Reticular Synthesis and the Design of New Materials. *Nature* **2003**, *423*, 705.
(30) Férey, G.; Serre, C. Large Breathing Effects in Three-Dimensional Porous Hybrid Matter: Facts, Analyses, Rules and Consequences. *Chem. Soc. Rev.* **2009**, *38*, 1380−1399.
(31) Inokuma, Y.; Kawano, M.; Fujita, M. Crystalline Molecular Flasks. *Nat. Chem.* **2011**, *3*, 349.
(32) Maji, T. K.; Matsuda, R.; Kitagawa, S. A Flexible Interpenetrating Coordination Framework with a Bimodal Porous Functionality. *Nat. Mater.* **2007**, *6*, 142.
(33) An, J.; Rosi, N. L. Tuning MOF CO2 Adsorption Properties via Cation Exchange. *J. Am. Chem. Soc.* **2010**, *132*, 5578−5579.
(34) Rix, D.; Ballesteros-Garrido, R.; Zeghida, W.; Besnard, C.; Lacour, J. Macrocyclization of Oxetane Building Blocks with Diazocarbonyl Derivatives under Rhodium (II) Catalysis. *Angew. Chem., Int. Ed.* **2011**, *50*, 7308−7311.
(35) Islamoglu, T.; Goswami, S.; Li, Z.; Howarth, A. J.; Farha, O. K.; Hupp, J. T. Postsynthetic Tuning of Metal−Organic Frameworks for Targeted Applications. *Acc. Chem. Res.* **2017**, *50*, 805−813.
(36) Yuan, S.; Zou, L.; Qin, J.-S.; Li, J.; Huang, L.; Feng, L.; Wang, X.; Bosch, M.; Alsalme, A.; Cagin, T.; et al. Construction of Hierarchically Porous Metal−Organic Frameworks Through Linker Labilization. *Nat. Commun.* **2017**, *8*, 15356.
(37) Cui, Y.; Li, B.; He, H.; Zhou, W.; Chen, B.; Qian, G. Metal−organic frameworks as Platforms for Functional Materials. *Acc. Chem. Res.* **2016**, *49*, 483−493.
(38) Liu, Y.; Kravtsov, V. C.; Larsen, R.; Eddaoudi, M. Molecular Building Blocks Approach to the Assembly of Zeolite-Like Metal−Organic Frameworks (ZMOFs) with Extra-Large Cavities. *Chem. Commun.* **2006**, *14*, 1488−1490.
(39) Uemura, T.; Yanai, N.; Watanabe, S.; Tanaka, H.; Numaguchi, R.; Miyahara, M. T.; Ohta, Y.; Nagaoka, M.; Kitagawa, S. Unveiling Thermal Transitions of Polymers in Subnanometre Pores. *Nat. Commun.* **2010**, *1*, 83.
(40) Nouar, F.; Eckert, J.; Eubank, J. F.; Forster, P.; Eddaoudi, M. Zeolite-like Metal−Organic Frameworks (ZMOFs) as Hydrogen Storage Platform: Lithium and Magnesium Ion-Exchange and H2-(rho-ZMOF) Interaction Studies. *J. Am. Chem. Soc.* **2009**, *131*, 2864−2870.
(41) Maiti, S.; Haupts, U.; Webb, W. W. Fluorescence Correlation Spectroscopy: Diagnostics for Sparse Molecules. *Proc. Natl. Acad. Sci. U. S. A.* **1997**, *94*, 11753−11757.
(42) Rigler, R.; Elson, E. S. *Fluorescence Correlation Spectroscopy: Theory and Applications*; Springer Science & Business Media: 2012; Vol. *65*.

DOI: 10.1021/acs.jpclett.8b02810
J. Phys. Chem. Lett. 2018, 9, 6399−6403